Monthly Notices
of the
ROYAL ASTRONOMICAL SOCIETY

MNRAS **430,** 3465–3471 (2013) doi:10.1093/mnras/stt147

CO(1–0) detection of molecular gas in the massive Spiderweb Galaxy ($z = 2$)*

B. H. C. Emonts,[1]† I. Feain,[1] H. J. A. Röttgering,[2] G. Miley,[2] N. Seymour,[1] R. P. Norris,[1] C. L. Carilli,[3] M. Villar-Martín,[4] M. Y. Mao,[3] E. M. Sadler,[5] R. D. Ekers,[1] G. A. van Moorsel,[3] R. J. Ivison,[6,7] L. Pentericci,[8] C. N. Tadhunter[9] and D. J. Saikia[10,11]

[1]*CSIRO Astronomy and Space Science, Australia Telescope National Facility, PO Box 76, Epping, NSW 1710, Australia*
[2]*Leiden Observatory, University of Leiden, PO Box 9513, NL-2300 RA Leiden, the Netherlands*
[3]*National Radio Astronomy Observatory, PO Box 0, Socorro, NM 87801-0387, USA*
[4]*Centro de Astrobiología (INTA-CSIC), Ctra de Torrejón a Ajalvir, km 4, E-28850 Torrejón de Ardoz, Madrid, Spain*
[5]*School of Physics, University of Sydney, NSW 2006, Australia*
[6]*UK Astronomy Technology Centre, Science and Technology Facilities Council, Royal Observatory, Blackford Hill, Edinburgh EH9 3HJ, UK*
[7]*Institute for Astronomy, University of Edinburgh, Blackford Hill, Edinburgh EH9 3HJ, UK*
[8]*INAF Osservatorio Astronomico di Roma, Via Frascati 33, I-00040 Monteporzio (RM), Italy*
[9]*Department of Physics and Astronomy, University of Sheffield, Sheffield S3 7RH, UK*
[10]*Cotton College State University, Panbazar, Guwahati 781 001, India*
[11]*National Centre for Radio Astrophysics, TIFR, Ganeshkhind, Pune 411 007, India*

Accepted 2013 January 23. Received 2013 January 23; in original form 2012 September 25

ABSTRACT

The high-redshift radio galaxy MRC 1138−262 ('Spiderweb Galaxy'; $z = 2.16$) is one of the most massive systems in the early Universe and surrounded by a dense 'web' of proto-cluster galaxies. Using the Australia Telescope Compact Array, we detected CO(1–0) emission from cold molecular gas – the raw ingredient for star formation – across the Spiderweb Galaxy. We infer a molecular gas mass of $M_{\rm H2} = 6 \times 10^{10}$ M$_\odot$ (for $M_{\rm H2}/L'_{\rm CO} = 0.8$). While the bulk of the molecular gas coincides with the central radio galaxy, there are indications that a substantial fraction of this gas is associated with satellite galaxies or spread across the intergalactic medium on scales of tens of kpc. In addition, we tentatively detect CO(1–0) in the star-forming proto-cluster galaxy HAE 229, 250 kpc to the West. Our observations are consistent with the fact that the Spiderweb Galaxy is building up its stellar mass through a massive burst of widespread star formation. At maximum star formation efficiency, the molecular gas will be able to sustain the current star formation rate (SFR ≈ 1400 M$_\odot$ yr^{-1}, as traced by Seymour et al.) for about 40 Myr. This is similar to the estimated typical lifetime of a major starburst event in infrared luminous merger systems.

Key words: galaxies: active – galaxies: clusters: individual: Spiderweb – galaxies: formation – galaxies: high-redshift – galaxies: individual: MRC 1138-262 – galaxies: ISM.

1 INTRODUCTION

High-z radio galaxies (HzRGs) are signposts of large overdensities in the early Universe, or proto-clusters, which are believed to be the ancestors of local rich clusters (e.g. Venemans et al. 2007; Miley & De Breuck 2008). Historically, HzRGs were often identified by the ultrasteep spectrum of their easily detectable radio continuum, which served as a beacon for tracing the surrounding faint proto-cluster (Röttgering et al. 1994; Chambers et al. 1996). HzRGs are typically the massive central objects in these proto-clusters.

One of the most impressive HzRGs is MRC 1138−262, also called the 'Spiderweb Galaxy' ($z = 2.16$; Pentericci et al. 1997; Miley et al. 2006). It is one of the most massive galaxies in the early Universe ($M_\star \sim 2 \times 10^{12}$ M$_\odot$; Seymour et al. 2007; De Breuck et al. 2010). The Spiderweb Galaxy is a conglomerate of star-forming clumps (or 'galaxies', following Hatch et al. 2009) that are embedded in a giant (>200 kpc) Lyα halo, located in the core of the Spiderweb proto-cluster (Pentericci et al. 1997; Carilli et al.

* From observations with the Australia Telescope Compact Array.
† E-mail: bjorn.emonts@csiro.au

1998, 2002). The central galaxy hosts the ultrasteep spectrum radio source MRC 1138−262 ($-1.2 \leq \alpha^{8.1\,\mathrm{GHz}}_{4.5\,\mathrm{GHz}} \leq -2.5$ for the various continuum components; Carilli et al. 1997; Pentericci et al. 1997). This source exerts dramatic feedback on to the Lyα gas (Nesvadba et al. 2006).

Emission-line surveys identified tens of galaxies to be associated with the Spiderweb Galaxy and its surrounding proto-cluster (Pentericci et al. 2000; Kurk et al. 2004; Croft et al. 2005; Doherty et al. 2010; Kuiper et al. 2011). These galaxies harbour a significant fraction of the system's unobscured star formation (Hatch et al. 2009). Overdensities of red sequence galaxies were found by Kodama et al. (2007) and Zirm et al. (2008). At Mpc scales, an overdensity of X-ray AGN traces a filamentary structure roughly aligned with the radio axis (Pentericci et al. 2002). Kuiper et al. (2011) showed that the proto-cluster is dynamically evolved and a possible merger of two subclusters. Hatch et al. (2009) predicted that most of the central proto-cluster galaxies will merge with MRC 1138−262 and double its stellar mass by $z = 0$, but that gas depletion will have exhausted star formation long before, so that the Spiderweb Galaxy will evolve into a cD galaxy found in the centres of present-day clusters.

Submillimetre (submm) observations showed that the Spiderweb has massive star formation extended on scales of >200 kpc (Stevens et al. 2003), in agreement with polycyclic aromatic hydrocarbon (PAH) emission from MRC 1138−262 and two Hα-emitting companions (Ogle et al. 2012). Despite significant jet-induced feedback (Nesvadba et al. 2006; Ogle et al. 2012), Seymour et al. (2012) derived a high star formation rate of SFR $\approx$ 1400 $\mathrm{M_\odot\ yr^{-1}}$ and an AGN accretion rate of 20 per cent of the Eddington limit for MRC 1138−262, indicating that it is in a phase of rapid growth of both black hole and host galaxy.

How long this phase will last and how much stellar mass will be added depends on the available fuel for the ongoing star formation. The raw ingredient for star formation (and potential AGN fuel) is molecular hydrogen (H_2). Extremely luminous mid-IR line emission from warm ($T > 300$ K), shocked H_2 gas has been detected in MRC 1138−262 with *Spitzer* (Ogle et al. 2012). This indicates that the radio jets may heat large amounts of molecular hydrogen, possibly quenching star formation in the nucleus (see Ogle et al. 2012 for a discussion). However, in order to fuel the observed large star formation rate (SFR), an additional extensive reservoir of cold molecular gas must be present. An excellent tracer of the cold component of H_2 is carbon monoxide, CO(*J, J–1*). Particularly efficient is the study of the ground-transition CO(1–0), which is the most robust tracer of the overall H_2 gas, including the widespread, low-density and subthermally excited component (Papadopoulos et al. 2000, 2001; Papadopoulos & Ivison 2002; Dannerbauer et al. 2009; Carilli et al. 2010; Ivison et al. 2011).

In this paper, we present the detection of CO(1–0) in the Spiderweb Galaxy. We assume $H_0 = 71$ km s^{-1} Mpc^{-1}, $\Omega_\mathrm{M} = 0.27$ and $\Omega_\Lambda = 0.73$ (i.e. angular distance scale of 8.4 kpc arcsec^{-1} and luminosity distance $D_\mathrm{L} = 17\,309$ Mpc).

2 OBSERVATIONS

CO(1–0) observations were performed with the Australia Telescope Compact Array (ATCA) during 2011 August to 2012 March in the compact hybrid H75 and H168 array configurations. The total on-source integration time was 22 h (after discarding data taken in poor weather, i.e. atmospheric path length rms fluctuations >400 μm; Middelberg, Sault & Kesteven 2006). Both 2 GHz ATCA bands were centred close to $\nu_\mathrm{obs} = 36.5$ GHz ($T_\mathrm{sys} \sim$ 70–100 K), corresponding to the redshifted CO(1–0) line. The phases and bandpass were calibrated every 5–15 min with a 2 min scan on the nearby bright calibrator PKS 1124-186. Fluxes were calibrated using Mars.

For the data reduction, we followed Emonts et al. (2011b). The relative flux-calibration accuracy between runs was $\lesssim$5 per cent, while the uncertainty in absolutely flux accuracy was up to 20 per cent based on the flux model for Mars (version 2012 March). The broad 2 GHz band ($\Delta v \approx 16\,000$ km s^{-1}) allowed us to separate the continuum from the line emission in the UV-domain by fitting a straight line to the line-free channels. We Fourier transformed the line data[1] to obtain a cube with robust weighting +1 (Briggs 1995), beam-size 9.54 arcsec × 5.31 arcsec (PA 63°.3) and channel width 8.6 km s^{-1}. The line data were binned by 15 channels and subsequently Hanning smoothed to a velocity resolution of 259 km s^{-1}, resulting in a noise level of 0.085 mJy beam^{-1} per channel.

The spectra presented in this paper were extracted against the central pixel in the regions described in the text (pixelsize 2.3 arcsec × 2.3 arcsec), unless otherwise indicated. Total intensity images of the CO(1–0) emission were made by summing the channels across which CO(1–0) was detected. All estimates of L'_CO in this paper have been derived from these total intensity images. The data were corrected for primary-beam attenuation ($\mathrm{FWHM_{PrimBeam}} =$ 77 arcsec) and are presented in optical barycentric velocity with respect to $z = 2.161$.

3 RESULTS

We detect CO(1–0) emission in the Spiderweb Galaxy (Fig. 1). The CO(1–0) profile appears double peaked, with a firm 5σ 'red' peak and tentative 3σ 'blue' peak, separated by ∼1000 km s^{-1}(with σ derived from the integrated line profile). Fig. 1 (*left*) shows a total intensity map of the red and blue component. The total ('red+blue') CO(1–0) emission-line luminosity that we derive is $L'_\mathrm{CO} = 7.2 \pm 0.6 \times 10^{10}$ K km s^{-1} pc^2 (following equation 3 in Solomon & Vanden Bout 2005).[2] Table 1 summarizes the CO(1–0) emission-line properties.

Fig. 1 (*left*) shows that the bulk of the CO(1–0) coincides with the radio galaxy (region 'B'). However, there are strong indications from both the gas kinematics and distribution that a significant fraction of the CO(1–0) emission is spread across tens of kpc.

First, despite the limited spatial resolution of our observations, there appears to be a velocity gradient in the gas kinematics across the inner 30–40 kpc of the Spiderweb. As shown in Fig. 1, the redshift of the CO(1–0) peak emission decreases when going from region 'A' to region 'B' to region 'C'. Most prominent is the apparent spatial separation between the peak of the blue component of the double-peaked CO(1–0) profile in region C and the peak of the red component in region B. Fig. 2 visualizes that also between regions B and A there is a clear velocity gradient in the CO(1–0) emission. The decrease in the velocity of the CO(1–0) peak emission from region A → B → C is consistent with a decrease in redshift of optical line-emitting galaxies found in these regions

[1] Similarly, we made a continuum map (10.39 arcsec × 6.55 arcsec, PA 75°.5). We detect the 36.6 GHz radio continuum with an integrated flux of $S_{36.6\,\mathrm{GHz}} = 10.7$ mJy ($P_{36.6\,\mathrm{GHz}} = 3.6 \times 10^{26}$ W Hz^{-1}) across three beam-sizes, following the morphology of high-resolution 4.7/8.2 GHz data of Carilli et al. (1997). A detailed discussion on the 36.6 GHz radio continuum is deferred to a future paper.

[2] The measurement error in L'_CO does not include a 20 per cent uncertainty in the model of our used flux calibrator Mars (Section 2).

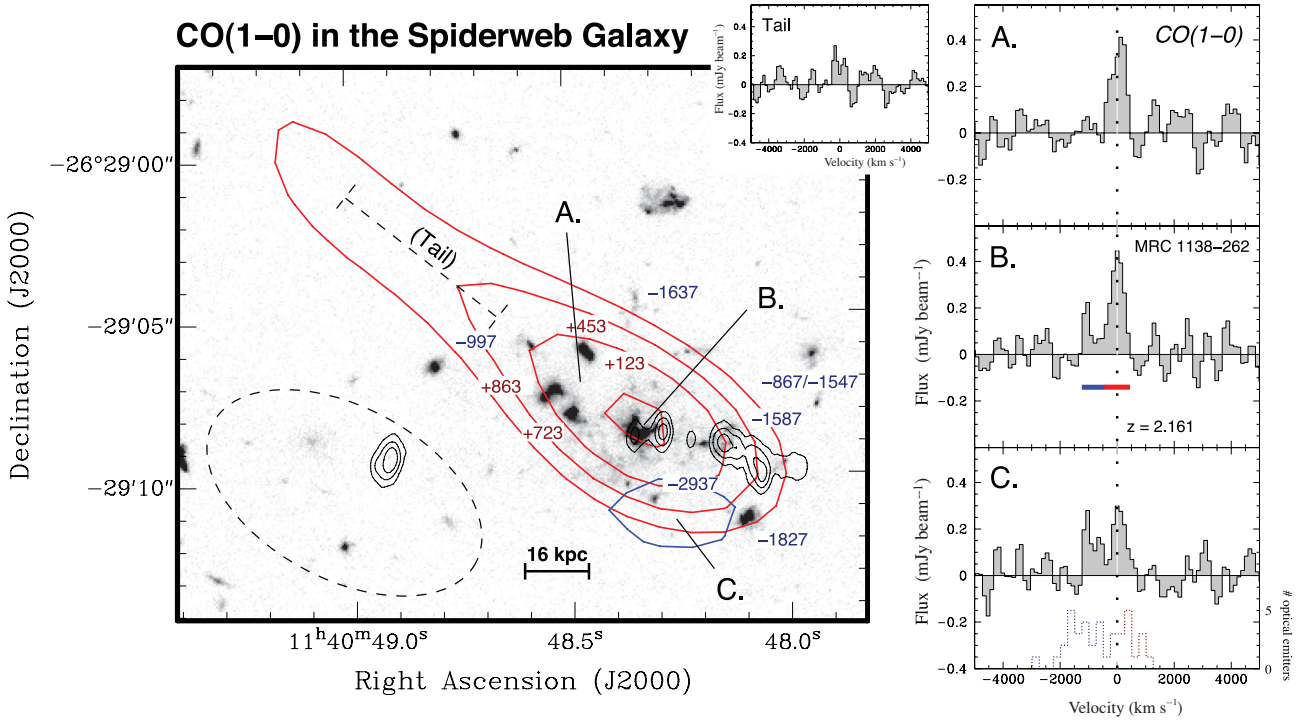

Figure 1. Left: contours of the CO(1–0) emission overlaid on to an *Hubble Space Telescope*/ACS (g_{475}+I_{814}) image of the Spiderweb Galaxy (Miley et al. 2006). The plot roughly equals the size of the giant Lyα halo (see Fig. 3), hence the individual galaxies shown here are part of the Spiderweb Galaxy. Contour levels of the CO(1–0) emission are 2.8, 3.5, 4.2 and 5.0σ (no negative contours are present at the same -2.8σ level, but see Fig. 3 for a larger field of view). The red and blue contours represent the red and blue part of the double-peaked CO(1–0) profile, as indicated by the horizontal bar in the right-middle plot (velocity ranges: red: $-453 < v < +453$ km s^{-1} with $\sigma = 0.046$ Jy beam^{-1} km s^{-1}; blue: $-1228 < v < -453$ km s^{-1} with $\sigma = 0.043$ Jy beam^{-1} km s^{-1}). Note that the blue signal is too weak to be detected across the FWHM of the synthesized beam, hence the emission and its exact location need to be verified with future observations. The black contours represent the 8.2 GHz radio continuum from Carilli et al. (1997). The dashed ellipse in the bottom-left corner shows the ATCA beam-size. The red and blue numbers indicate the velocities of individual galaxies as derived from optical emission lines (adjusted for $z = 2.161$; Kuiper et al. 2011). Right: CO(1–0) emission-line profiles at four different regions within the Spiderweb Galaxy. The apertures of regions A, B and C are described in Section 2. The spectrum of the tentative NE tail was taken by averaging 4 pixels along the dashed line in the left plot. Although the profiles are not mutually independent, they suggest that there is a change in the CO(1–0) kinematics across the regions A, B and C. The velocity is centred on $z = 2.161$ (Section 3). The dotted histogram in the bottom plot shows the distribution of optical and UV rest-frame line emitters in the Spiderweb Galaxy and surrounding proto-cluster (from Kuiper et al. 2011).

Table 1. CO(1–0) properties in the various regions of the Spiderweb Galaxy and HAE 229: $z_{CO(1-0)}$ = redshift, $v_{CO(1-0)}$ = velocity of the peak emission w.r.t $z_{CO(1-0)} = 2.161$; FWHM = CO(1–0) line width at half the maximum intensity; FWZI = full width of the CO(1–0) profile at zero intensity; S_ν (peak) = CO peak flux; $I_{CO(1-0)}$ = CO integrated flux; $L'_{CO(1-0)}$ = CO total intensity: M_{H2} = H_2 mass (Section 4.1). z, v, FWHM and S_ν have been derived from Gaussian fits to the CO profiles in Figs 1 and 3. $I_{CO(1-0)}$, $L'_{CO(1-0)}$ and M_{H2} have been derived from the total intensity images in Figs 1 and 3.

		Spiderweb Galaxy (SG)			HAE 229
		SG region A	SG region B	SG region C	
$z_{CO(1-0)}$		2.163 ± 0.001	2.161 ± 0.001	2.150 ± 0.001	2.147 ± 0.001
$v_{CO(1-0)}$	(km s^{-1})	175 ± 75	0 ± 30	-1060^{+185}_{-40}	-1355 ± 65
FWHM	(km s^{-1})	550^{+165}_{-210}[a]	540 ± 65	550^{+150}_{-300}[a]	395 ± 75
FWZI	(km s^{-1})	905 ± 130 (A + B)[b]		775 ± 130	520 ± 130
S_ν(peak)	(mJy beam^{-1})	0.44 ± 0.06	0.44 ± 0.06	0.30 ± 0.09	0.32 ± 0.05
$I_{CO(1-0)}$	(Jy km s^{-1})	0.28 ± 0.03 (A + B)[b]		0.03 ± 0.01	0.14 ± 0.01
$L'_{CO(1-0)}$	($\times 10^{10}$ K km s^{-1} pc^2)	6.5 ± 0.6 (A + B)[b]		0.7 ± 0.2	3.3 ± 0.2
M_{H2}	($\times 10^{10}$ M$_\odot$)	5 ± 1 (A + B)[b]		0.6 ± 0.2	3 ± 1

[a]Values are quoted for a single Gaussian profile fit, with errors reflecting uncertainties due to asymmetry of the corresponding profile component.
[b]Regions A and B are spatially unresolved and only marginally resolved kinematically, hence a single value is derived from the entire 'red' part of the total intensity image of Fig. 1.

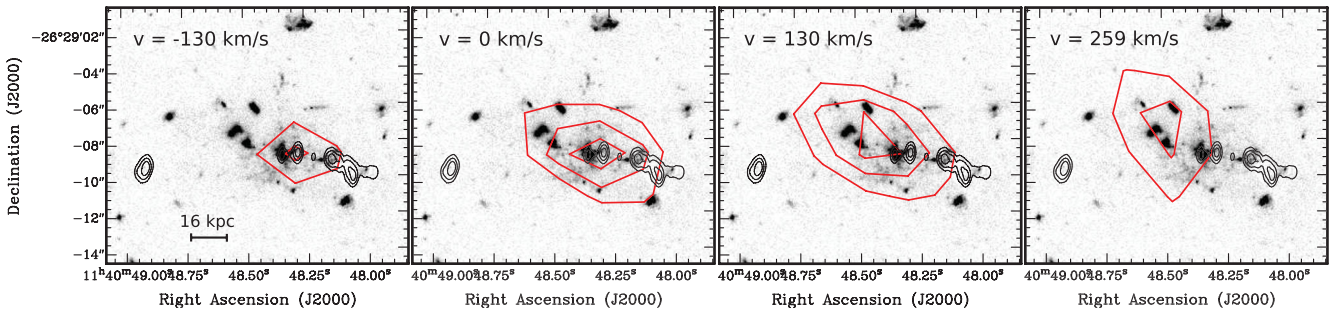

Figure 2. Channel maps of the CO(1–0) emission in regions A and B, highlighting a gradient in the gas kinematics. Contour levels of the CO(1–0) emission (red) are 3.0, 3.8 and 4.5σ (with $\sigma = 0.085$ mJy beam^{-1}; Section 2). No negative features are present in these channels at the same level (-3σ). The radio continuum (black contours), beam-size and redshift are the same as in Fig. 1.

(see Fig. 1, though note that the large ATCA beam prevents us from spatially resolving the individual galaxies in our CO data). Fig. 1 also shows indications for an extension ('tail') of the CO(1–0) emission beyond region A (stretching up to 100 kpc NE of the radio core), but this tail is detected only at a 3σ level and thus needs to be verified. We have started an observational programme to verify the distribution and kinematics of the CO(1–0) emission at higher sensitivity and spatial resolution (results will be reported in a future paper).

In addition, the double-peaked CO(1–0) profile spreads over 1700 km s^{-1} (FWZI). This is extreme compared to what is found for quasars and submm-galaxies (see Coppin et al. 2008; Wang et al. 2010; Ivison et al. 2011; Riechers et al. 2011; Bothwell et al. 2013; Krips, Neri & Cox 2012 and references therein). A few notable exceptions are high-z systems in which the broad CO profiles arise from merging galaxies (Salomé et al. 2012 and references therein). As can be seen in Fig. 1 (*bottom right*), the double-peaked CO profile resembles the velocity distribution of optical line emitters detected in the Spiderweb proto-cluster (Kuiper et al. 2011), be it with a lower velocity dispersion of the CO gas, in particular on the blueshifted side.

These results thus indicate that a significant fraction of the CO(1–0) detected in the Spiderweb Galaxy likely originates from (merging) satellites of the central radio galaxy, or the intergalactic medium (IGM) between them.

Our results also suggests that the redshift of the central radio galaxy is associated with the red peak of the CO(1–0) profile, giving $z_{\rm CO(1-0)} = 2.161 \pm 0.001$. Kuiper et al. (2011) discuss that determining the redshift from optical and UV rest-frame emission lines is bound to a much larger uncertainty, but they derive $2.158 < z < 2.170$, which is in agreement with our estimated $z_{\rm CO(1-0)}$.

3.1 HAE 229

Fig. 3 shows that also the dusty star-forming galaxy HAE 229 ($M_\star \sim 5 \times 10^{11}$ M$_\odot$; Kurk et al. 2004; Doherty et al. 2010) is detected in CO(1–0) at 3.7σ significance. We derive $L'_{\rm CO} = 3.3 \pm 0.2 \times 10^{10}$ K km s^{-1} pc^2 for HAE 229. Table 1 summarizes the CO(1–0) properties. HAE 229 is located 250 kpc (30 arcsec) West of MRC 1138−262, i.e. outside the giant Lyα halo. The CO(1–0) signal peaks at $v = -1354$ km s^{-1}, which agrees with the Hα redshift from Kurk et al. (2004). None of the other line-emitting

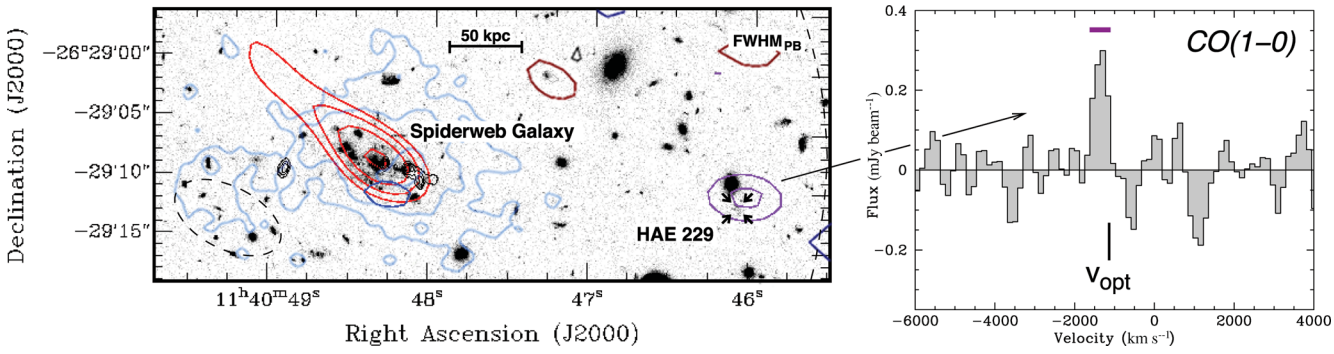

Figure 3. Left: the Spiderweb Galaxy and HAE 229. Shown is a zoom-out of Fig. 1 (*left*) including the CO(1–0) contours of HAE 229 (purple) 250 kpc to the West. The light-blue contours indicate the extent of the Lyα halo that encompasses the Spiderweb Galaxy (from Miley et al. 2006, see also Pentericci et al. 1997). The red and blue contours are the same as in Fig. 1 (2.8, 3.5, 4.2 and 5.0σ), with σ the noise level at the phase centre (centred on the Spiderweb Galaxy). The dark-red and dark-blue contours are the corresponding negative signal (present only at -2.8σ at a significant distance from the phase centre, where the noise increases due to correction of the signal for primary-beam attenuation). Contour levels of the CO(1–0) in HAE 229 are -2.8 (grey), 2.8 and 3.5σ (purple), derived across the velocity range indicated by the purple bar in the spectrum on the right ($-1618 < v < -1100$ km s^{-1}; $\sigma = 0.048$ Jy beam^{-1} × km s^{-1}). For HAE 229, σ is the local rms noise (i.e. 30 arcsec from the phase centre) in the primary-beam-corrected total intensity CO image. The dashed partial circle on the right shows the FWHM of the primary beam (i.e. the effective field of view) of our observations. The small arrows indicate the location of a peak in 24 μm emission that coincides with HAE 229 (data from De Breuck et al. 2010). Right: CO(1–0) spectrum of HAE 229. The systemic velocity, as derived from optical emission lines, is also indicated (Kurk et al. 2004). Note that the higher noise in this spectrum compared to the spectra of Fig. 1 is a result of the primary-beam correction.

galaxies outside the Lyα halo, but within the field of view of our observations, is reliably detected in CO(1–0).

4 DISCUSSION

4.1 Molecular gas in the Spiderweb

We can estimate the mass of molecular gas by adopting a standard conversion factor $\alpha_x = M_{H2}/L'_{CO} = 0.8$ [$M_\odot$ (K km s^{-1} pc^2)$^{-1}$] (where M_{H2} includes a helium fraction; e.g. Solomon & Vanden Bout 2005). This is consistent with α_x found in ultraluminous infrared galaxies ($L_{IR} > 10^{12}$ L$_\odot$; Downes & Solomon 1998), but we stress that the conversion from L'_{CO} into M_{H2} is not yet well understood (Tacconi et al. 2008; Ivison et al. 2011) and that α_x crucially depends on the properties of the gas, such as metallicity and radiation field (Glover & Mac Low 2011). Adopting $\alpha_x = 0.8$ $M_\odot$ (K km s^{-1} pc^2)$^{-1}$ results in an estimated molecular gas mass in the Spiderweb Galaxy of $M_{H2} \sim 6 \times 10^{10}$ M$_\odot$. We argue that this is likely a conservative estimate, based on the adopted conversion factor and the fact that a large amount of shock-heated molecular gas resides in the warm ($T > 100$ K) phase (see Ogle et al. 2012). The putative H_2 mass of HAE 229 is $M_{H2} \sim 3\times10^{10}$ M$_\odot$.

4.1.1 Nature of the molecular gas

In Section 3, we saw that, while the CO(1–0) distribution is concentrated on the central radio galaxy, the CO emission spreads across the inner 30–40 kpc (a region which is rich in satellite galaxies). Based on its distribution and kinematics, we argued that part of the molecular gas is thus most likely associated with these satellite galaxies or the IGM between them. The extreme FWZI of the CO(1–0) emission (Section 3) is another indication that the double-peaked profile is not likely caused by a nuclear disc in the central radio galaxy. This is consistent with earlier speculation by Ogle et al. (2012) that the high SFR could be the result of the accretion of gas or gas-rich satellites (which were found by Hatch et al. 2009 to contain most of the dust-uncorrected, instantaneous star formation), while nuclear star formation may be quenched by jet-induced heating of the molecular gas.

The tentative NE tail (see Fig. 1) spreads further out, beyond region A (which is rich in satellite galaxies) into a region with no known companion galaxies or detectable Lyα emission (Fig. 3). However, a Mpc-scale filamentary structure exists in the east–west direction (Pentericci et al. 2002). We speculate that – if confirmed – this tentative tail might indicate that cold gas is found, or being accreted along, this filament.

Two alternative scenarios that should be considered to explain the CO characteristics are AGN-driven outflows and cooling flows. Cooling flows have been detected in CO in giant central cluster (cD) galaxies at $z < 0.4$, some of which contain H_2 masses similar to that of the Spiderweb Galaxy. However, compared to the Spiderweb Galaxy, these cooling flow galaxies show much narrower typical line widths (FWHM$_{CO}$ < 500 km s^{-1}, taking into account an uncertain α_x and the use of narrow-band receivers; Edge 2001; Salomé & Combes 2003; Salomé et al. 2006). Radio-jet-driven outflows of optical emission-line gas were found on scales of tens of kpc in the Spiderweb Galaxy by Nesvadba et al. (2006). Similar to the CO distribution, these optical emission lines are significantly more redshifted NW compared to SE of the radio core, though the ambiguity in optical redshifts makes a direct comparison difficult. Still, there is an interesting alignment between the redshifted CO(1–0) emission in region A and the region in which Nesvadba et al. (2006) detect the fastest redshifted outflow velocities in the optical emission-line gas (their 'zone 1', which stretches in between region A and B). The FWHM of the optical emission-line gas is, however, significantly larger than that of the CO(1–0) emission, indicating that it has a much larger velocity dispersion. Both the cooling flow and the radio-jet feedback scenario deserve further investigation, once CO observations with higher resolution and sensitivity have confirmed the extent of the CO(1–0) emission.

4.2 Evolutionary stage

From fitting the mid- to far-IR spectral energy distribution, Seymour et al. (2012) derive a starburst IR luminosity of $L_{IR} = 8 \times 10^{12}$ L$_\odot$ and star formation rate of SFR = 1390 M$_\odot$ yr^{-1} for MRC 1138−262. $L_{IR}/L'_{CO(1-0)}$ agrees well with correlations found in various types of low- and high-z objects (e.g. Ivison et al. 2011). Assuming that all the H_2 is available to sustain the high SFR, we derive a minimum mass depletion time-scale of $t_{depl} = \frac{M_{H2}}{SFR} \approx 40$ Myr. This is comparable to the estimated typical lifetime of a major starburst episode in IR-luminous merger systems (Mihos & Hernquist 1994; Swinbank et al. 2006), though the bulk of the intense star formation in the Spiderweb Galaxy may occur on scales of tens of kpc (Section 4.1.1). The mass depletion time-scale may be shorter if the cold molecular gas is more rapidly depleted by feedback processes, such as shock-heating (Ogle et al. 2012) or jet-induced outflows (found to occur at rates of ∼400 M$_\odot$ yr^{-1} in the optical emission-line gas by Nesvadba et al. 2006). Nevertheless, both the current large SFR and cold molecular gas content imply that we are witnessing a phase of rapid galaxy growth though massive star formation, coinciding with the AGN activity.

The H_2 mass is much larger than the estimated mass of the emission-line gas in the Lyα halo ($M_{emis} = 2.5 \times 10^8$ M$_\odot$; Pentericci et al. 1997). However, Carilli et al. (2002) show that the radio source is enveloped by a region of hot, shocked X-ray gas of potentially $M_{hot} = 2.5 \times 10^{12}$ M$_\odot$. This suggests that, even when the current reservoir of cold molecular gas is consumed, there is a potential gas reservoir available for future episodes of starburst (and AGN) activity, provided that the gas can cool down to form molecular clouds (e.g. Fabian 1994) and this process is not entirely counteracted by ongoing AGN feedback (Carilli et al. 2002; Nesvadba et al. 2006; Ogle et al. 2012). The merger of proto-cluster galaxies with the Spiderweb Galaxy may also trigger a new burst of star formation, depending on the available gas reservoir in these systems.

For the dusty star-forming galaxy HAE 229, $L'_{CO(1-0)}$ is comparable to that of IR-selected massive star-forming galaxies at $z = 1.5$ (Aravena et al. 2010) and some high-z submm galaxies (e.g. Ivison et al. 2011). Our CO results are consistent with observations by Ogle et al. (2012) that HAE 229 is going through a major and heavily obscured starburst episode. From their calculated SFR ∼ 880 M$_\odot$ yr^{-1}, we derive $t_{depl} \approx 30$ Myr, i.e. similar to that of the Spiderweb Galaxy.

4.3 CO(1–0) in HzRGs

MRC 1138−262 is part of an ATCA survey for CO(1–0) in a southern sample of HzRGs ($1.4 < z < 3$; Emonts et al in preparation, see also Emonts et al. 2011a,b). So far, it is one of only very few secure CO(1–0) detections among HzRGs; two other examples being

MRC 0152−209 ($z = 1.92$; Emonts et al. 2011a) and 6C 1909+72 ($z = 3.53$; Ivison et al. 2012).

CO detections in HzRGs made with narrow-band receivers and/or higher transitions are also still limited in number (Scoville et al. 1997; Alloin, Barvainis & Guilloteau 2000; Papadopoulos et al. 2000, 2001; De Breuck et al. 2003a, 2005; De Breuck, Neri & Omont 2003b; Greve, Ivison & Papadopoulos 2004; Klamer et al. 2005; Ivison et al. 2008, 2012; Nesvadba et al. 2009; Emonts et al. 2011b, also review by Miley & De Breuck 2008). However, in some cases CO is resolved on tens of kpc scales (Ivison et al. 2012), associated with various components (e.g. merging gas-rich galaxies; De Breuck et al. 2005), or found in giant Lyα haloes that surround the host galaxy (Nesvadba et al. 2009). This shows that detectable amounts of cold molecular gas in HzRGs are not restricted to the central region of the radio galaxy. Ivison et al. (2012) discuss that CO-detected HzRGs (often pre-selected on bright far-IR emission from a starburst) are generally associated with merger activity. This is also the case for the Spiderweb Galaxy, which is located in an extreme merger environment.

Using the Jansky Very Large Array (JVLA), Carilli et al. (2011) mapped CO(2–1) emission throughout a $z = 4$ proto-cluster associated with the submm galaxy GN20 (tracing a combined mass of $M_{\rm H2} \sim 2 \times 10^{11}$ M$_\odot$). Our results on the Spiderweb Galaxy and HAE 229 are another example of the potential for studying the lowest CO transitions in proto-cluster environments with the ATCA and JVLA.

5 CONCLUSIONS

We detect CO(1–0) emission from cold molecular gas across the massive Spiderweb Galaxy, a conglomerate of star-forming galaxies at $z = 2.16$. While the bulk of the CO(1–0) coincides with the central radio galaxy, part of the molecular gas is spread across tens of kpc. We explain that this gas is most likely associated with satellites of the central radio galaxy, or the IGM between them (though other scenarios are briefly discussed). The extensive reservoir of cold molecular gas likely provides the fuel for the widespread star formation that has been observed across the Spiderweb Galaxy. Continuous galaxy-merger and gas-accretion processes are the likely triggers for the observed high SFR. The total mass of cold gas ($M_{\rm H2} = 6 \times 10^{10}{}_{[\alpha_x=0.8]}$ M$_\odot$) is enough to sustain the current high SFR in the Spiderweb Galaxy for ∼40 Myr, which is similar to the typical lifetime of major starburst events seen in IR-luminous merger systems. Our CO results on the Spiderweb Galaxy show the potential for studying the cold gas throughout high-z proto-clusters with the ATCA, JVLA and Atacama Large Millimeter/submillimeter Array.

ACKNOWLEDGEMENTS

We thank Ernst Kuiper for sharing his *HST* imaging and the anonymous referee for useful feedback that improved this paper. We also thank the Narrabri observatory staff for their help. BE acknowledges the Centro de Astrobiología/INTA for their hospitality. NS is recipient of an ARC Future Fellowship. The Australia Telescope is funded by the Commonwealth of Australia for operation as a National Facility managed by CSIRO.

REFERENCES

Alloin D., Barvainis R., Guilloteau S., 2000, ApJ, 528, L81
Aravena M. et al., 2010, ApJ, 718, 177
Bothwell M. S. et al., 2013, MNRAS, 429, 3047
Briggs D. S., 1995, PhD thesis, New Mexico Tech
Carilli C. L., Roettgering H. J. A., van Ojik R., Miley G. K., van Breugel W. J. M., 1997, ApJS, 109, 1
Carilli C. L., Harris D. E., Pentericci L., Rottergering H. J. A., Miley G. K., Bremer M. N., 1998, ApJ, 494, L143
Carilli C. L., Harris D., Pentericci L., Röttgering H., Miley G., Kurk J., van Breugel W., 2002, ApJ, 567, 781
Carilli C. L. et al., 2010, ApJ, 714, 1407
Carilli C. L., Hodge J., Walter F., Riechers D., Daddi E., Dannerbauer H., Morrison G. E., 2011, ApJ, 739, L33
Chambers K. C., Miley G. K., van Breugel W. J. M., Huang J.-S., 1996, ApJS, 106, 215
Coppin K. E. K. et al., 2008, MNRAS, 389, 45
Croft S., Kurk J., van Breugel W., Stanford S. A., de Vries W., Pentericci L., Röttgering H., 2005, AJ, 130, 867
Dannerbauer H., Daddi E., Riechers D. A., Walter F., Carilli C. L., Dickinson M., Elbaz D., Morrison G. E., 2009, ApJ, 698, L178
De Breuck C. et al., 2003a, A&A, 401, 911
De Breuck C., Neri R., Omont A., 2003b, New Astron. Rev., 47, 285
De Breuck C., Downes D., Neri R., van Breugel W., Reuland M., Omont A., Ivison R., 2005, A&A, 430, L1
De Breuck C. et al., 2010, ApJ, 725, 36
Doherty M. et al., 2010, A&A, 509, A83
Downes D., Solomon P. M., 1998, ApJ, 507, 615
Edge A. C., 2001, MNRAS, 328, 762
Emonts B. H. C. et al., 2011a, ApJ, 734, L25
Emonts B. H. C. et al., 2011b, MNRAS, 415, 655
Fabian A. C., 1994, ARA&A, 32, 277
Glover S. C. O., Mac Low M., 2011, MNRAS, 412, 337
Greve T., Ivison R., Papadopoulos P., 2004, A&A, 419, 99
Hatch N. A., Overzier R. A., Kurk J. D., Miley G. K., Röttgering H. J. A., Zirm A. W., 2009, MNRAS, 395, 114
Ivison R. J. et al., 2008, MNRAS, 390, 1117
Ivison R. J., Papadopoulos P., Smail I., Greve T., Thomson A., Xilouris E., Chapman S., 2011, MNRAS, 412, 1913
Ivison R. J. et al., 2012, MNRAS, 425, 1320
Klamer I. J., Ekers R. D., Sadler E. M., Weiss A., Hunstead R. W., De Breuck C., 2005, ApJ, 621, L1
Kodama T., Tanaka I., Kajisawa M., Kurk J., Venemans B., De Breuck C., Vernet J., Lidman C., 2007, MNRAS, 377, 1717
Krips M., Neri R., Cox P., 2012, ApJ, 753, 135
Kuiper E. et al., 2011, MNRAS, 415, 2245
Kurk J. D., Pentericci L., Overzier R. A., Röttgering H. J. A., Miley G. K., 2004, A&A, 428, 817
Middelberg E., Sault R., Kesteven M., 2006, PASA, 23, 147
Mihos J. C., Hernquist L., 1994, ApJ, 431, L9
Miley G., De Breuck C., 2008, A&AR, 15, 67
Miley G. K. et al., 2006, ApJ, 650, L29
Nesvadba N. P. H., Lehnert M. D., Eisenhauer F., Gilbert A., Tecza M., Abuter R., 2006, ApJ, 650, 693
Nesvadba N. P. H. et al., 2009, MNRAS, 395, L16
Ogle P., Davies J. E., Appleton P. N., Bertincourt B., Seymour N., Helou G., 2012, ApJ, 751, 13
Papadopoulos P. P., Ivison R. J., 2002, ApJ, 564, L9
Papadopoulos P., Röttgering H., van der Werf P., Guilloteau S., Omont A., van Breugel W., Tilanus R., 2000, ApJ, 528, 626
Papadopoulos P., Ivison R., Carilli C., Lewis G., 2001, Nat, 409, 58
Pentericci L., Roettgering H. J. A., Miley G. K., Carilli C. L., McCarthy P., 1997, A&A, 326, 580
Pentericci L. et al., 2000, A&A, 361, L25
Pentericci L., Kurk J. D., Carilli C. L., Harris D. E., Miley G. K., Röttgering H. J. A., 2002, A&A, 396, 109
Riechers D. A. et al., 2011, ApJ, 739, L32
Roettgering H. J. A., Lacy M., Miley G. K., Chambers K. C., Saunders R., 1994, A&AS, 108, 79
Salomé P., Combes F., 2003, A&A, 412, 657
Salomé P. et al., 2006, A&A, 454, 437

Salomé P., Guélin M., Downes D., Cox P., Guilloteau S., Omont A., Gavazzi R., Neri R., 2012, A&A, 545, A57
Scoville N. Z., Yun M. S., Windhorst R. A., Keel W. C., Armus L., 1997, ApJ, 485, L21
Seymour N. et al., 2007, 171, 353
Seymour N. et al., 2012, ApJ, 755, 146
Solomon P. M., Vanden Bout P. A., 2005, ARA&A, 43, 677
Stevens J. A. et al., 2003, Nat, 425, 264
Swinbank A. M., Chapman S. C., Smail I., Lindner C., Borys C., Blain A. W., Ivison R. J., Lewis G. F., 2006, MNRAS, 371, 465
Tacconi L. J. et al., 2008, ApJ, 680, 246
Venemans B. P. et al., 2007, A&A, 461, 823
Wang R. et al., 2010, ApJ, 714, 699
Zirm A. W. et al., 2008, ApJ, 680, 224

This paper has been typeset from a TEX/LATEX file prepared by the author.